

Use of Computer Graphic Simulation to Explain Color Histogram Structure

Liang Peng, Eric P. F. Lafortune, Donald P. Greenberg
Cornell University Program of Computer Graphics, Ithaca, NY
Irwin Sobel
Printing Technology Department, Hewlett Packard Laboratories, Palo Alto, CA

Abstract

In this paper, we discuss the use of computer graphics techniques to model and explain the structures commonly observed in color histograms of images. This includes an accurate simulation of the physical reflection and transport behavior of light energy within 3D environments, the precise modeling of an image capturing system, and an interactive visualization module to display color histograms. Based on the fundamental rendering equation that describes light reflection and transport in the 3D world, we classify the color histogram structures of color images, and relate them to various physical components in image formation, including scene illumination, material reflectance properties, and the surface geometry of objects. We further show how these histogram structures can be effected by the artifacts caused by the limitation of image capturing systems. Our results demonstrate that the use of accurate simulation procedures under a precisely controlled computer graphic environment can clearly illustrate the causes of the structures observed, and can provide unique insights and explanations of image formation.

1. Introduction

Color histograms have been widely used in many image processing and computer vision systems. The structures observed in color histograms contain shading and shadow information of the 3D scene, and are used as important cues of physical processes for image analysis and object recognition [9, 8, 2, 12]. Previous research is mainly based on a dichromatic reflection model [13], consisting of two components, surface reflection (e.g. specular reflection) and body reflection (e.g. diffuse reflection) [13, 9, 8]. The dichromatic model has been demonstrated to be successful in some computer vision systems to recognize and separate these two reflection components for image segmentation purpose [8, 2, 12]. However, commonly used approaches do not directly account for the indirect illumination from other surfaces, and hence can not describe the color histogram structures evident in scenes with indirect lighting. Bajcsy and Lee [3] extended this model by considering the first order of inter-reflection among surfaces. To date, no research has been published on the structures in the color histogram resulting from the more general effects of global illumination, an illumination model that includes the indirect lighting from all the surfaces with multiple reflections in the 3D scene.

In this work, we have shown that with well controlled, physically accurate computer graphic simulations, where the light reflection and transport processes are fully characterized with spectral and spatial information, we are able to not only reproduce the realistic images with the color histogram features reported by early researchers, but also produce images with more complex features such as the off-plane thickening and "banana" shaped structures in the color histograms by incorporating the effects of global illumination.

2. Color Image Formation

2.1. Image Capture

In a digital image CCD capturing system, the measured image irradiance value at location (x, y) of a pixel array is:

$$I(x,y) = T \int_{\lambda} \hat{I}(x,y,\lambda) S(\lambda) d\lambda \qquad (1)$$

where T is the total exposure time, $\hat{I}(x, y, \lambda)$ is the spectral irradiance entering the camera and falling on the pixel area at (x, y) in the detector plane [1], and $S(\lambda)$ is the spectral response function of the sensor. The sensor device usually has three channels with different spectral response curves, yielding a triplet measurement, (r, g, b) at each (x, y) position. This is the input data for our color histogram analysis system.

Since we have used a pinhole camera model for the image capture system, it is a idealized imaging device with an infinitely small aperture, no vignetting effect, and perfect focusing. For a real camera with a lens of finite aperture,

[1] For the illustration purpose, the physical dimension of a pixel is first ignored. Later, this restriction is removed, and the effect of area integration within a pixel is considered.

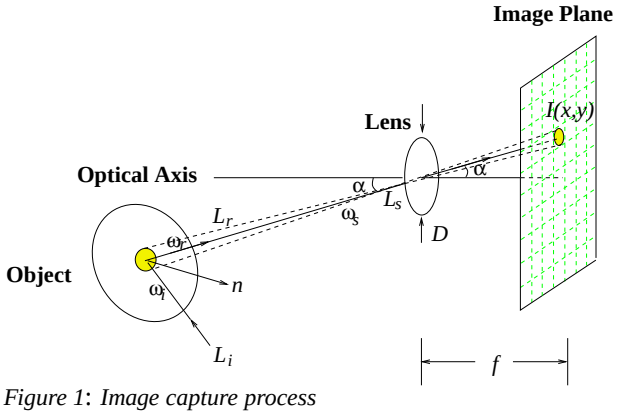

Figure 1: *Image capture process*

the incident spectral irradiance at (x, y) is proportional to the spectral radiance ($L_s(\hat{\omega}_s, \lambda)$) in the scene [6]:

$$\hat{I}(x, y, \lambda) = \frac{\pi}{4}(\frac{D}{f})^2 cos^4\alpha \cdot L_s(\hat{\omega}_s, \lambda) \qquad (2)$$

Here, as shown in Figure 1, $\hat{\omega}_s$ is the direction of a light ray entering the aperture of the camera and landing at (x, y), D and f are the aperture diameter and image distance of the camera respectively, and α is the angle between the directions of the incoming light ray and the optical axis of the camera. The triplet measurement is then: [2]

$$\begin{pmatrix} r(x,y) \\ g(x,y) \\ b(x,y) \end{pmatrix} = \begin{pmatrix} \langle R(\lambda), I(x,y,\lambda)\rangle \\ \langle G(\lambda), I(x,y,\lambda)\rangle \\ \langle B(\lambda), I(x,y,\lambda)\rangle \end{pmatrix} \qquad (3)$$

where $R(\lambda)$, $G(\lambda)$, and $B(\lambda)$ are the three basis functions which represent the combined effects of :

1. The optical spectral transfer function of the camera, and the spatial off-axis attenuation due to lens vignetting.
2. The spectral responses and quantum efficiency of CCD sensors.
3. The combined conversion factor from photon numbers to electron numbers, electron numbers to voltage readouts, and finally from voltage readouts to pixel values.
4. The integration over time for the duration of the exposure.

Combining the above two equations, we get

$$\begin{pmatrix} r \\ g \\ b \end{pmatrix} = \frac{\pi}{4}(\frac{D}{f})^2 cos^4\alpha \begin{pmatrix} \langle R(\lambda), L_s(\hat{\omega}_s, \lambda)\rangle \\ \langle G(\lambda), L_s(\hat{\omega}_s, \lambda)\rangle \\ \langle B(\lambda), L_s(\hat{\omega}_s, \lambda)\rangle \end{pmatrix} \qquad (4)$$

[2]Here, we use *Dirac*'s bracket notation to express the inner product in the L_2 space. e.g. For any real function $g(\lambda)$ and $f(\lambda)$, $\langle g(\lambda), f(\lambda)\rangle = \int_0^\infty g(\lambda)f(\lambda)d\lambda$.

Note that $L_s(\hat{\omega}_s, \lambda)$, the spectral radiance in the scene imaged at (x, y) in the focal plane includes the spectral radiance coming not only directly from the emitting light sources, but also indirectly from the reflecting surfaces. Equation (4) illustrates a direct correspondence between (r, g, b) and $L_s(\hat{\omega}_s, \lambda)$, where the distribution of (r, g, b) forms a color histogram in RGB space.

2.2. Rendering Equation and Light Transport

The spectral radiance in the scene can be theoretically calculated by solving the rendering equation: [7, 1]

$$L_s(\hat{\omega}_s, \lambda) = L_e(\hat{\omega}_s, \lambda) + \int_{\Omega_i} \rho(\hat{\omega}_i, \hat{\omega}_r, \lambda)\ (\hat{n}\cdot\hat{\omega}_i)\ L_i(\hat{\omega}_i, \lambda) d\hat{\omega}_i \qquad (5)$$

Here, $L_e(\hat{\omega}_s, \lambda)$, is the illumination entering the camera directly from the light source. $L_i(\hat{\omega}_i, \lambda)$ is the incident spectral radiance on a surface of interest, $\hat{n}$ is the normal direction of the surface, $\hat{\omega}_i$ and $\hat{\omega}_r$ are the directions of the incident and reflected light respectively. Notice that $\hat{\omega}_s$ is the same direction as $\hat{\omega}_r$, but measured in the coordinate of the camera. Ω_i is the integration domain of $\hat{\omega}_i$, and ρ is the bidirectional reflectance distribution function (BRDF). The BRDF specifies the reflectance property of the surface material of an object and is a function of $\hat{\omega}_i$, $\hat{\omega}_r$ and λ.

Based on the theory of global illumination, the incident illumination on each surface can be represented as:

$$L_i(\hat{\omega}_i, \lambda) = L_i^{(0)}(\hat{\omega}_i, \lambda) + L_i^{(1)}(\hat{\omega}_i, \lambda) + L_i^{(2)}(\hat{\omega}_i, \lambda) + \cdots \qquad (6)$$

where, $L_i^{(0)}(\hat{\omega}_i, \lambda)$ is the direct illumination term from the light source in the direction $\hat{\omega}_i$; All the other terms $L_i^{(k)}$ are the result of indirect illumination from all the other surfaces after the light has k bounces.

There are two net effects on the light after it is reflected from a surface: its intensity is attenuated, and its spectrum composition is changed. Both of these two are attributed to the BRDF of the surface from which it is reflected. Hence, the indirect lighting has a different spectrum than the direct lighting, which is due to the modulation by the spectral component of the BRDF. The attenuation factor of intensity is a geometric term, which is usually in an integral form that depends on the spatial component of the BRDF and the orientation of the surface.

In the dichromatic model [13], the BRDF consists of two components, ρ_s, the specular component corresponding to the surface layer reflections, and ρ_d, the diffuse component corresponding to the reflections at sub-surface layers. In many materials such as plastics, the index of refraction changes very little over the visible spectrum, so ρ_s can be approximated with a flat spectrum and does not change the spectral composition of the incident light, while in general ρ_d does.[8] Here, we adopt a more generic form

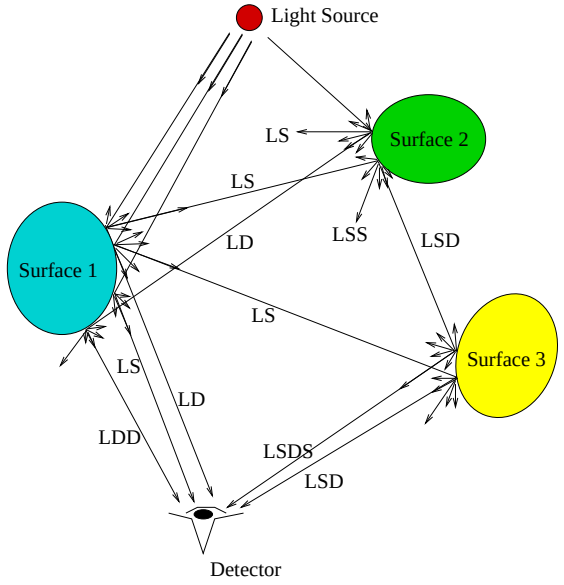

Figure 2: *Light path under multiple reflections*

of a physically based BRDF, where ρ_d may include a directional diffuse component in additional to the Lambertian homogeneous component [4], and may have spatial variations. However, both components are assumed to be separable in spatial and spectral terms. In order to clarify how light changes its spectral composition at each reflecting surface, we ignore the geometric terms, and introduce the following LSD symbolic notation [3] to represent the color of the light along its possible light propagation paths: (Figure 2)

- $L = \langle \mathbf{C}, \mathbf{L^{(0)}} \rangle$: directly from the light source.
- $LD = \langle \mathbf{C}, \rho_\mathbf{d} \mathbf{L^{(0)}} \rangle$: after being reflected once from a diffuse surface
- $LS = \langle \mathbf{C}, \rho_\mathbf{s} \mathbf{L^{(0)}} \rangle$: after being reflected once from a specular surface
- $LDD = \langle \mathbf{C}, \rho_\mathbf{d} \rho_\mathbf{d} \mathbf{L^{(0)}} \rangle$: after being consecutively reflected from two diffuse surfaces
- $LSS = \langle \mathbf{C}, \rho_\mathbf{s} \rho_\mathbf{s} \mathbf{L^{(0)}} \rangle$: after being consecutively reflected from two specular surfaces
- $LSD = \langle \mathbf{C}, \rho_\mathbf{d} \rho_\mathbf{s} \mathbf{L^{(0)}} \rangle$: after being reflected from a specular surface and then a diffuse surface.
- $LDS = \langle \mathbf{C}, \rho_\mathbf{s} \rho_\mathbf{d} \mathbf{L^{(0)}} \rangle$: after being reflected from a diffuse surface and then a specular surface.

[3] This notation is based on an article by Heckbert [5]

Here $\mathbf{C}$ is used to represent $(R, G, B)^T$, and $\mathbf{I}$ is the triplet $(r, g, b)^T$. We then get

$$\begin{aligned} \mathbf{I} &= L + L(D+S) \\ &+ L(D+S)D + L(D+S)S \\ &+ L(D+S))DD + L(D+S)DS \\ &+ L(D+S)SD + L(D+S)SS + \cdots \end{aligned} \quad (7)$$

In this notation, each appended D or S may be considered as diffuse reflection or specular reflection operators acting on the string (resulting spectral radiance of light) to the left of it. This shows that the final colors in an image consist of components produced at all levels of reflection. If ρ_s has a flat spectral composition, the specular reflection light path only changes the magnitude of the illumination color, while all diffuse reflection light paths in general modify both the magnitude and the direction of the light color. The total amount of the color change is a cumulative effect of all the reflections on the light path before the light enters the camera.

3. Analysis of structures in color histograms

3.1. Features from physical reflection process

Based on the LSD notation from the last section, we now present an analytic understanding of the structures in color histograms:

We first examine the color histogram structures under the direct illumination condition. This occurs when the incident radiance on any surface in the scene comes only directly from light sources. (1) When the BRDF of a surface only consists of a diffuse component ρ_d, the reflected light has only the LD component which contains the shading information, and generates a linear cluster in RGB space((a) in Figure 3). (2) When the BRDF of a surface consists of both a diffuse component ρ_d and a specular component ρ_s, the reflected light now has the color contribution from both LS and LD, samples of which span a planar subspace in the RGB space. [4] For smooth surfaces, ρ_s may change very fast near the specular peak direction of ω_r, leading to the situation where the majority of the color values lie mainly on the LD vector, with only a small portion having a significant specular component, and veering sharply towards the LS direction, forming a L-shaped structure. When the specular region is more extended, a P-shaped structure may result instead. ((b) in Figure 3). (3) When multiple luminaires with different spectra are present in the scene, the total spectral radiance in the scene is the superposition of the spectral radiances from each single lumi-

[4] In the case of ρ_s has flat spectrum, LS is in the same direction as L in RGB space since the S operation does not change the direction of the illumination color, the plane is actually defined by the vectors L and LD.

naire, leading to a superposition of the cluster structures in the color histogram.

The properties of color histogram structures change when global illumination is considered. In the situation where there is only one light source present in the scene, and each surface has only a diffuse BRDF component, the color values resulting from global illumination have contributions from all levels of diffuse reflection LD_i, LD_iD_j $LD_iD_jD_k$, etc $\cdots$. The cumulative effect of all these reflection colors in general yields a much more complicated volume structure. One interesting consequence is that even if all the surfaces are made of the same material with the same reflectance properties, as long as the diffuse reflection does not have a flat spectrum, each reflection changes the spectral composition of the incident light, and modifies the direction of the resulting color in the RGB space by rotating (r,g,b) through a small angle. [5] In most situations, the reflected light energy drops very quickly after the first few bounces on the surfaces, and one observes a thickening effect in many histogram features. ((c) in Figure 3). Sometimes, fork-like structures may also be formed due to the fact that more than one other reflecting surface dominates the indirect lighting. Furthermore, when the specular component of BRDF is also included with the global illumination, the resulting color values have contributions from all levels of diffuse and specular reflections LD_i, LS_i, LD_iD_j, LS_iD_j, LD_iS_j, LS_iS_j, etc $\cdots$, and the L-shaped or P-shaped features are also thickened or "corrupted" by the indirect illumination. The cumulative effect of the successive rotations at all levels generates a curved structure corresponding to the "banana" feature frequently observed in color histograms. ((d) in Figure 3).

3.2. Artifacts from image capture process

Artifacts caused by the limitation of the imaging system also explain features observed in color histograms: (1) Due to the finite size of a pixel, the (r, g, b) value recorded at pixel location (x, y) is actually an integrated triplet quantity over the area of this pixel. Thus a pixel may have a color value which is averaged among several objects that it covers. This introduces some interpolated structures between existing color clusters. (2) Many image capturing systems record a non-linear response to the incoming light energy to compensate for the human perception system. This response is usually characterized by a power function, $I' = kI^{\gamma}$, whereas the exponent γ is commonly known as the gamma factor. This non-linear mapping causes distortion in the histogram structures, although the linear clusters are preserved under such a mapping. (3) Pixel values can also be saturated due to the limited dynamic range of the detector device. This yields clipping features in color space, where at least one of the three values of (r, g, b) reaches its maximal value, and remains at this value while other components keep changing. Lastly, noise in the image capture process has many sources. The dark current (DC) and any constant level bias will only cause a shift of the histogram structures in the RGB space. However, uniformly distributed quantization noise, Gaussian distributed readout noise, and Poisson distributed shot noise can cause thickening of the histogram structures. Most of these effects are illustrated in Figure 4.

[5] This is a form of von Kries transformation [14] rather than a rotation, but the change to the chromaticity is effectively the same as a rotation, and we no longer distinguish them.

4. Experiments and Results

We have used a Monte Carlo based bidirectional path tracing rendering system to produce physically accurate synthetic images in a controlled lighting environment[10]. Our simulation system supports the reflectance model for simple Lambertian surfaces, dichromatic surfaces with Phong lighting model, as well as realistic BRDF models based on physical measurements [4, 11]. We have built an interactive image segmentation and recognition system to select a color consistent region in the image plane, and display its 3D color histogram in the RGB space. The system also allows us to identify and measure the shape and orientation of a selected color cluster in the color space. Based on this information, we can make further inferences about the reflectance of objects as well as measure the illumination colors in the image.

For this paper, we have used a test environment composed of a box with a ceiling, a floor and three walls, containing a cylinder and a sphere. There is an illumination source on the ceiling. In order to fully understand and explain the structures in the color histogram space, we have adopted a multi-step procedure in the image formation and analysis process. We first synthesize images with only a Lambertian reflectance model under direct lighting, and examine the structures in the color space. Then we progressively add more components into the image formation process by assigning different reflectance spectra to the objects in the scene, adding specular reflection into the BRDF, changing the spectral composition of the luminaire, having more than one spectrally distinct luminaires in the scene, and having global illumination in the image synthesis. All of the images are computed with a full spectral range before the final projection to the RGB space. By examining and comparing the new features with the old structures in the color histogram, we are able to correlate the structures in the color histogram with the physical components in the lighting reflection process in image formation.

To understand how the color histogram structures are effected by the limitations of an imaging system, the partial

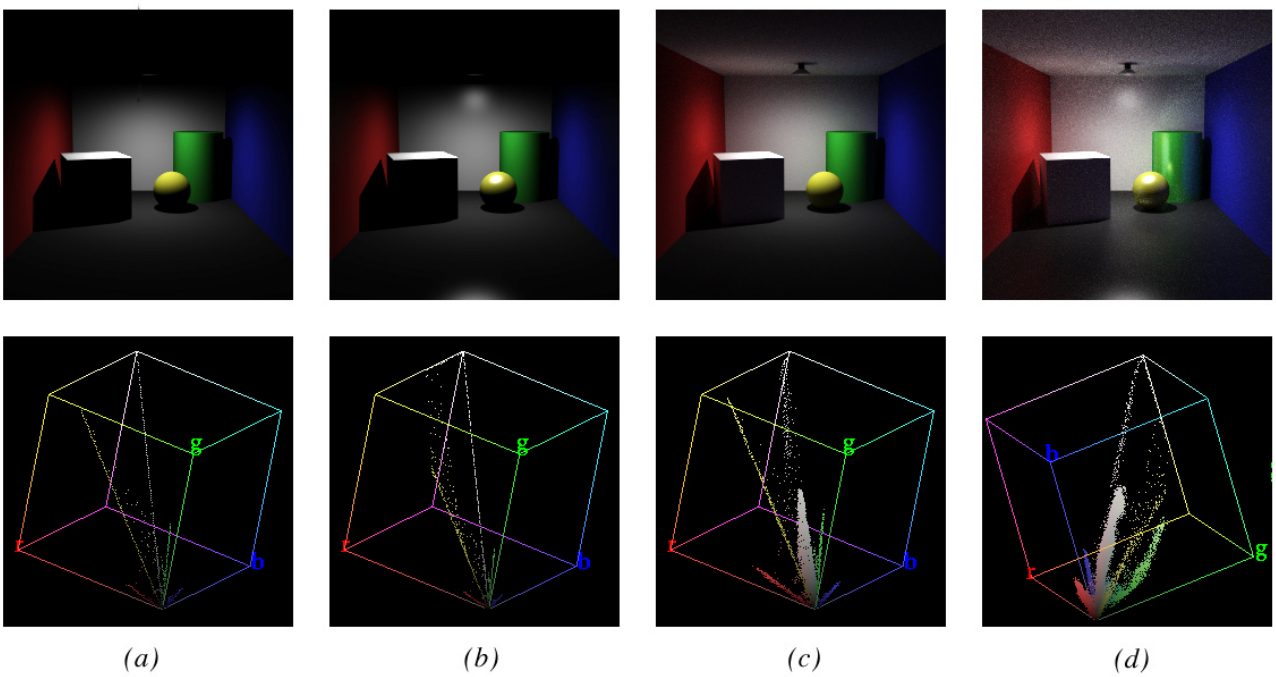

Figure 3: *Simulations of Color histogram. From left to right are: (a) Diffusely reflecting surfaces under direct illumination, (b) Dichromatically reflecting surfaces under direct illumination, (c) Diffusely reflecting surfaces under global illumination, (d) Dichromatically reflecting surfaces under global illumination.*

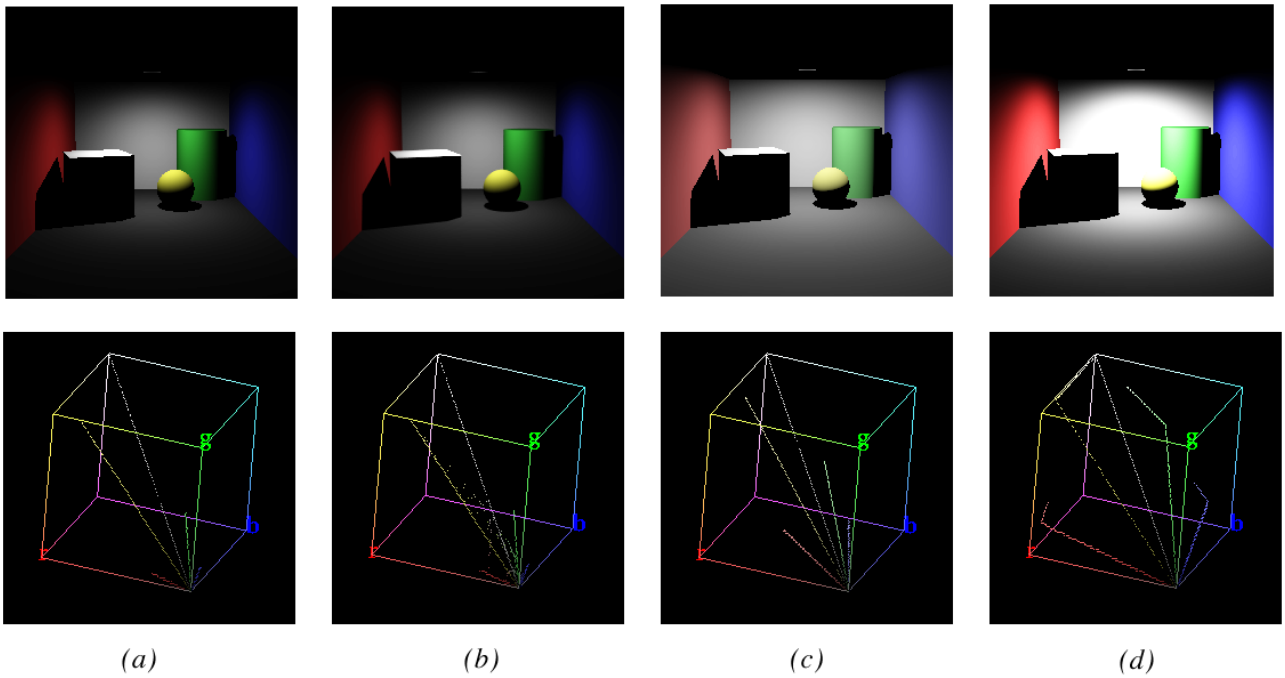

Figure 4: *Histograms of images with direct illumination. From left to right are: (a) Original image. (b) With supersampling in the area of a pixel. (c) With a different gamma factor. (d) With clipping effect by over exposure.*

pixel effect is simulated by super-sampling the pixels with multiple rays. Further more, the effects of limited dynamic range, gamma correction, and random noise in the detector are also modeled. [6]

5. Summary and Future Work

We have presented comprehensive analyses and explanations of the structures commonly observed in color histograms of color images based on the physics of light interactions with the surfaces in three dimensional environment. By using physically accurate, precisely controlled computer graphic simulation environment, we have been able to isolate and explain the formation of these structures. In order to elucidate the correspondence between the physical components of image formation, and the structures in the color histogram, we have adopted a progressive approach in the process of image formation and color histogram analysis. Using a dichromatic reflection model in our synthetic image generation system, we have successfully reproduced images with predicted features (linear clusters, T-shaped clusters, P-shaped clusters) in the color histogram under direct illumination. These clusters are caused by the superposition of the two components of the reflection from objects' surfaces, and have been observed in previous research [9, 2]. Furthermore, we have also produced more complex new features such as off-plane thickening and "banana" shaped structures in the color histogram by incorporating the global illumination model in our image synthesis. Future work needs to consider more complex BRDF's. Although our experiments have been conducted in an accurate computer graphic simulation environment, physical measurements are needed to validate our model and support our results.

Acknowledgements

We are thankful to Hewlett-Packard Corporation for their support of this research. We also thank Steve Marschner for his suggestions and help in our software development.

References

[1] J. Arvo. Transfer equations in global illumination. In *Global Illumination, SIGGRAPH 93 Course Notes*, volume 42, August 1993.

[2] R. Bajcsy, S. W. Lee, and A Leonardis. Color image segmentation with detection of highlights and local illumination induced by inter-reflection. In *Proc. 10th International Conf. on Pattern Recognition*, pages 785–790, 1990.

[3] R. Bajcsy, S. W. Lee, and A Leonardis. Detection of diffuse and specular interface reflections and inter-reflections by color image segmentation. *International Journal of Computer Vision*, 17(3):241–272, 1996.

[4] X.D. He, K.E. Torrance, F.X. Sillion, and D.P. Greenberg. A comprehensive physical model for light reflection. In *Computer Graphics*, pages 175–186, July 1991.

[5] P. S. Heckbert. Adptive radiosity textures for bidirectional ray tracing. In *Computer Graphics*, pages 145–154, 1990.

[6] B. K. P. Horn and R. W. Sjoberg. Calculating the reflectance map. In B. K. P. Horn and M. J. Brooks, editors, *Shape from Shading*, pages 215–244. The MIT Press, Cambridge, Massachusetts, 1989.

[7] J. Kajiya. The rendering equation. In *Computer Graphics*, pages 143–150, August 1986.

[8] G. J. Klinker. *A Physical Approach to Color Image Understanding.* A K Peters, Ltd, Wellesley, MA, 1993.

[9] G. J. Klinker, S. A. Shafer, and T. Kanada. A physical approach to color image understanding. *International Journal of Computer Vision*, 4(1):7–38, 1990.

[10] E.P. Lafortune. *Mathematical Models and Monte Carlo Algorithms for Physically Based Rendering, PhD Dissertation.* Katholieke Universiteit Leuven, feb 1996.

[11] Eric P. F. Lafortune, Sing-Choong Foo, Kenneth E. Torrance, and Donald P. Greenberg. Non-linear approximation of reflectance functions. In *Computer Graphics*, volume 31, August 1997.

[12] S. W. Lee and R. Bajcsy. Detection of specularity using color and multiple views. *Image and Vision Computing*, 10:643–653, 1992.

[13] S. A. Shafer. Using color to separate reflection components. *COLOR research and application*, 10(4):210–218, 1985.

[14] G. Wyszecki and W. S. Stiles. *Color Science: Concepts and Methods, Quantitative Data and Formulae.* Jhon Wiley & Sons, Inc, 1982.

[6] Please note that due to the restriction of black and white reproduction of this Proceedings, we can only illustrate a portion of our results here.